Proceedings of the 23rd International Congress on Applications of Lasers and Electro-Optics 2004

THE USE OF REACTIVE GAS SHIELDING FOR PRODUCTION OF HARD COATINGS BY LASER SURFACE ALLOYING

S. S. Babu[1], S. M. Kelly[2,3], M. Murugananth[4], R. P. Martukanitz[5]

[1] Metals and Ceramics Division, Oak Ridge National Laboratory, Oak Ridge, TN 37831
[2]Joint Institute of Computational Sciences, Oak Ridge National Laboratory, Oak Ridge, TN 37831
[3]Department of Materials Science and Engineering, Virginia Tech, Blacksburg, VA 24061
[4]School of Materials Engineering, Nanyang Technological University, Singapore 639798
The Applied Research Laboratory, State College, PA 16801

Abstract

A computational thermodynamic model was used to guide the generation of composite hard coatings made of hard particles distributed uniformly in a steel matrix. The calculations suggested that precipitation of titanium carbonitrides in liquid steel could be achieved by increasing the supersaturation of carbon, nitrogen and titanium in liquid steel. This condition was achieved by nitrogen addition to shielding gas during laser surface alloying while laser melting and solidifying a mixture of 431-type stainless steel and titanium carbide powders. With 100% nitrogen shielding deposits exhibited increased hardness compared to that of 100% argon shielding.

Introduction

Laser surface alloying (LSA) of steel involves localized melting of an alloy with a laser beam and the addition of alloying or second phase constituents, which in this case involves the formation of a composite coating through the addition of hard particles including carbides, nitrides and borides. On cooling to room temperature, these hard particles are trapped in the steel matrix and lead to better properties [1–12]. The properties of the LSA region depend on the microstructure that evolves during melting and cooling. Previous work has attempted to control LSA microstructure by modifying the laser beam parameters and by changing the alloying additions through extensive experimental research [13, 14]. The current work pertains to the application of computational thermodynamic models to design new laser surface alloy materials and processing parameters.

Most LSA processing has been performed with inert gas shielding to avoid oxidation of metal through reaction with oxygen, and also to avoid formation of pores due to excessive dissolution of nitrogen. Research in self-shielded flux cored arc welding has shown that a large concentration of dissolved nitrogen in a steel weld does not always lead to the formation of pores. In this case, porosity formation was avoided because the nitrogen reacts with dissolved aluminum in the steel [15–19]. Therefore, it was hypothesized that one can extend the same principle to the laser surface alloying process and achieve finer distribution of carbides or nitrides by using a reactive gas shielding methodology.

Garcia et al [20] employed 100% nitrogen shielding during laser surface alloying titanium samples. In many instances, the industrial practice for laser surface alloying is to avoid oxygen and nitrogen dissolution during laser surface alloying of ferrous materials to minimize the tendency for gas porosity [21]. Nevertheless, it is possible to fix the nitrogen by reacting with dissolved titanium to form nitrides, thereby avoiding the formation of porosity. It is also well known that titanium in the steel can also react with carbon to form titanium carbide. In the presence of both carbon and nitrogen, the titanium carbonitrides can also form.

Theoretical Calculations

In this study, the relative tendency to form carbides, nitrides and carbonitrides are evaluated with computational thermodynamic models to design a better alloy mixture. In this work, we used ThermoCalc® software [22] with the ThermoTech-Iron database [23] to calculate relative phase stability of carbides, nitrides and carbonitrides as a function of titanium, carbon and nitrogen concentration. Since titanium carbide and titanium carbonitride all have similar face centred cubic crystal structure, in the calculations they are represented by MX, where M stands for metal atom and X for either carbon or nitrogen or both.

In the first step, the tendency for MX formation as a function of titanium and carbon with no dissolved nitrogen was calculated at 1800 K [see Fig, 1*a*] for a simple Fe-C-Ti-N alloy system. The calculations showed that to form MX (titanium carbide) the

titanium concentration has to be greater than 1.9 wt.% and the carbon concentration has to be greater than 6.9 wt.%.

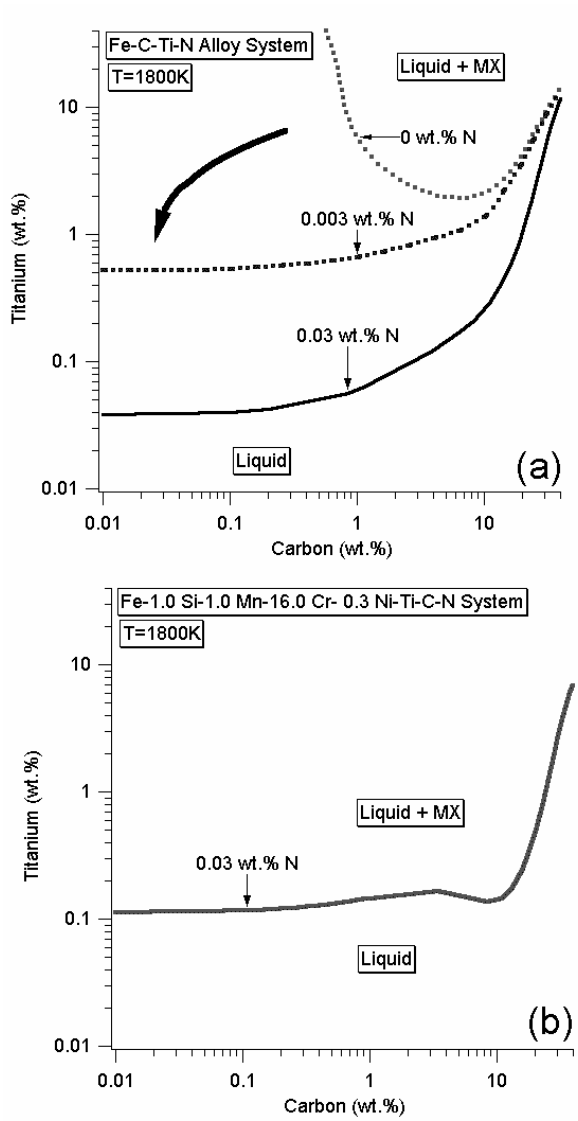

Fig. 1. Calculated phase stability of MX phase in liquid steel as a function of titanium, carbon and nitrogen concentration in (*a*) model Fe-C-Ti-N system the arrows indicate the direction of solubility line above which the formation of MX phase is favoured with an increase in nitrogen concentration and (*b*) Fe-Si-Mn-Cr-Ni-Ti-C-N system.

In the next step, the effect of dissolved nitrogen was considered. The stability of MX phase increased with an increase concentration of nitrogen in the liquid steel [see Fig. 1*a*].

The plots show that the MX phase forms at low carbon concentration for a given titanium concentration. The calculations also indicated that the MX phases under these conditions are titanium-rich carbonitrides. These calculations suggested that by dissolving titanium, carbon and nitrogen the precipitation of fine hard particles in liquid steel could be promoted. It is important to note the Fe-C-Ti-N matrix system is too simplistic and not typical to real industrial practice. Therefore, in the third step, similar calculations were performed with a 431 steel matrix (Fe-Si-Mn-Cr-Ni-Ti-C-N) as a base system and the effect of titanium, carbon and nitrogen were calculated and these results are shown in Fig. 1*b*. The addition of Cr, Si, Ni and Mn slightly modified the stability of MX phase; however, the calculations supported the notion of increased stability of MX phase through simultaneous addition of carbon, nitrogen and titanium. The validity of these calculations was evaluated by the following experimentation.

Materials and Methods

Materials: A commercially pure 431 steel powder (Sulzer-Metco 42C powder) was used as the matrix material. The nominal composition of the 431steel was Fe-0.2C-1Si-1Mn-16Cr (wt. %). A TiC powder of 99% purity was obtained from AEE Corporation. In this experiment, 80 wt.% 431 steel powder was mixed with 20 wt.% TiC powder and pre-placed to a thickness of 2 mm on a 1020-mild steel substrate having a nominal composition Fe-0.2C-0.5Mn (wt.%).

Nd-YAG Laser Surface Alloying: The laser deposition was made using a Hobart Model HLP 3000 3.0 kW Nd-YAG laser with fiber optic beam delivery and f16 focus optics. The beam diameter was 5 mm and the angle of the laser source was 15° rear angle. A laser power of 2430 W was used in all experiments. In all the experiments, the powder material to be melted by the laser process was premixed and pre-placed on the substrate surface. The width of the pre-placed powder layer was approximately 1.5 cm. Shielding gases were delivered to the laser surface processing region through a 9.5 mm inside diameter copper nozzle at 30° reverse angle from the direction of processing.

Diode Laser Surface Alloying: In order to scale up the process for wide surfaces the similar experiments were performed with different laser source. A Nuvonyx direct diode laser with a power setting of 4.0 kW was used. The heat source dimension was set at 12 mm width and 0.8 mm depth. The travel velocity was set at 4.2 mm/s to avoid excessive build up. The same powder mixture (80 wt. % 431 steel powders were mixed with 20 wt. % TiC powders) was delivered to the laser melted area at a rate of 25 gram per minute.

The shielding gas was provided at a flow rate of 40 cfh (19 l/min) from both sides of the deposition. The overlap of each pass was set at 6 mm.

Microstructure Characterization: The laser bead shape and microstructure in the deposits were characterized using optical microscopy after standard preparation and etching. The hardness distributions in the coatings were measured with an automated hardness tester (Buehler Micromet 2001 hardness tester equipped with the Omnimet Advantage software). The hardness measurements were performed at equal intervals of 200 µm with 300-gram loads and were presented in terms of Vickers Hardness Number (HV).

Results and Discussions

The deposit bead shapes obtained under different conditions are shown in Fig. 2*a* to 2*d*. Interestingly, increased nitrogen content in shielding-gas has lead to shallower beads than with 100% argon shielding. This result also shows that the dilution of base metal is reduced under this condition. Previous calorimetric analysis showed that the maximum process efficiency for both single and multi-bead process conditions was 70% [24]. However, subtle changes in this process efficiency with different shielding gases were not measured. The bead shape will also be governed by the modification of fluid flow conditions due to Marangoni stresses [25,26].

Optical microstructure from the deposits produced with various shielding gas conditions is presented in Fig. 3. The microstructures show in all conditions, carbide particles were present. With addition of TiC to the powder mixture, all of the samples showed the presence of a fine distribution of carbide particles [see Fig. 3*a* to 3*d*]. Interestingly, even without any gas shielding, a fine distribution of carbides could be observed [see Fig. 3*c*]. The shape of these carbides in all the samples varied from facetted, well rounded, and small dendritic. The microstructure showed that the carbide morphology was predominantly dendritic. Detailed analysis also showed that the dendritic shape of carbide particles with nitrogen-shielded deposits is well developed compared to argon shielding, suggesting that they formed at high temperature and had sufficient time to grow.

The results are in agreement with computational thermodynamic calculations. Although, X-ray diffraction analysis from the deposits indicated the presence of a face centered cubic crystal structure, it is difficult to distinguish whether they are carbides or nitrides without further high-resolution characterization. Since the dendritic structure was developed in the nitrogen condition, we can only speculate that these are titanium carbonitrides.

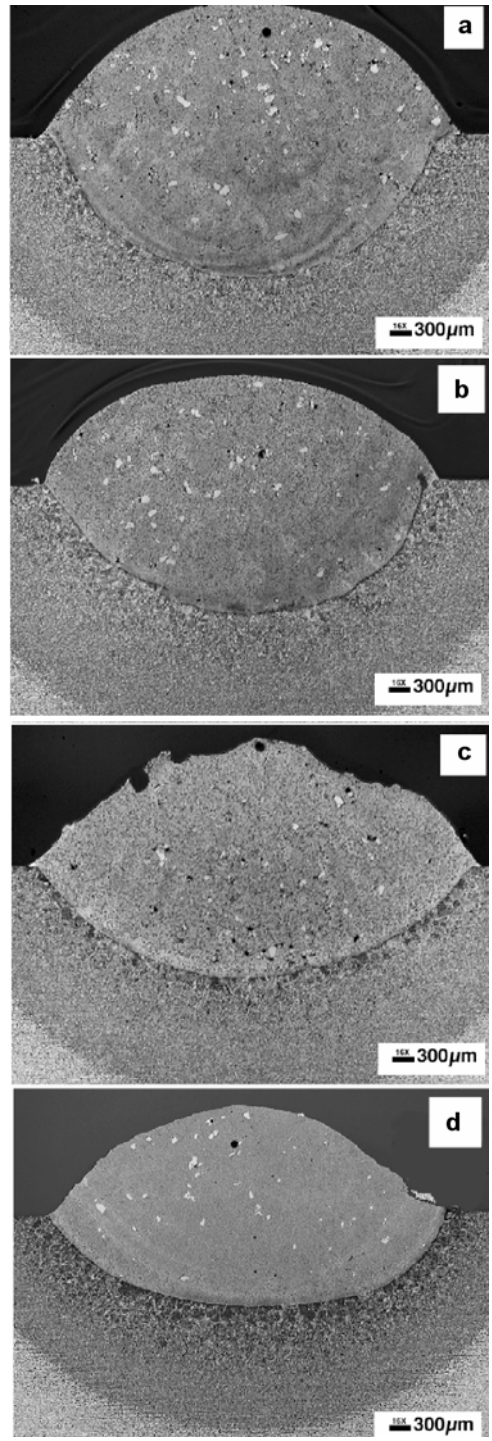

Fig. 2. Comparison of deposit shapes under different conditions: (*a*) 80 wt.% 431 – 20wt.%TiC – 20cfh Ar Shielding; (*b*) 80 wt.% 431 – 20 wt.% TiC – 18cfh Ar mixed with 2cfh N_2 Shielding; (*c*) 80 wt.% 431 – 20 wt.% TiC – No Shielding; and (*d*) 80 wt.% 431 – 20 wt.% TiC – 20cfh N_2 Shielding.

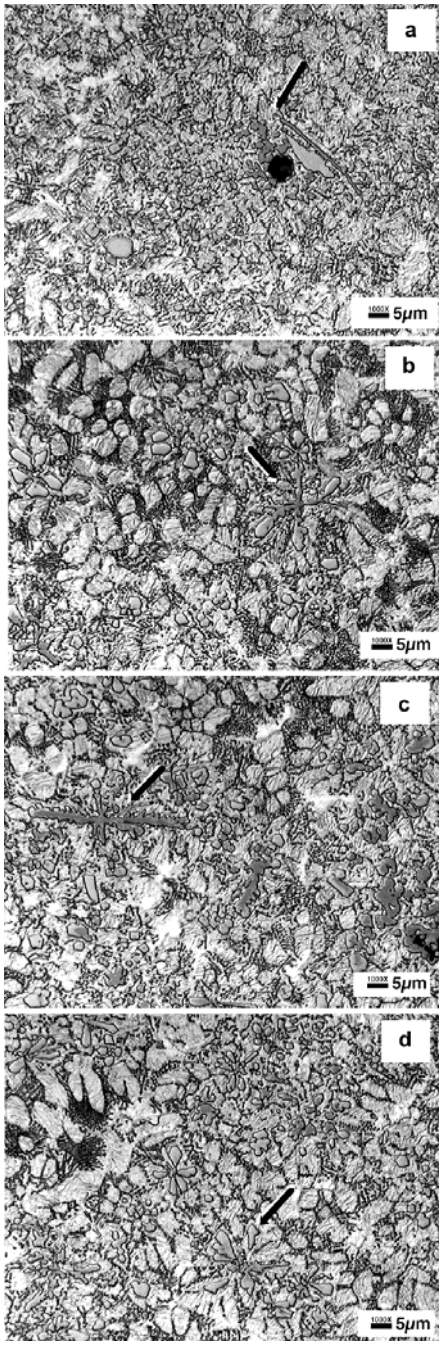

Fig. 3. Optical microstructure from deposits: (*a*) 80 wt.% 431 – 20wt.%TiC – 20cfh Ar Shielding; (*b*) 80 wt.% 431 – 20 wt.% TiC – 18cfh Ar mixed with 2cfh N_2 Shielding; (*c*) 80 wt.% 431 – 20 wt.% TiC – No Shielding; and (*d*) 80 wt.% 431 – 20 wt.% TiC – 20cfh N_2 Shielding. Arrows in the micrographs indicate typical carbides in the deposit.

In order to evaluate whether the variation in microstructure produced by changing the shielding gas conditions leads to a variation of mechanical properties, spatial hardness measurements were made in all four deposits and the results are presented in Fig. 4.

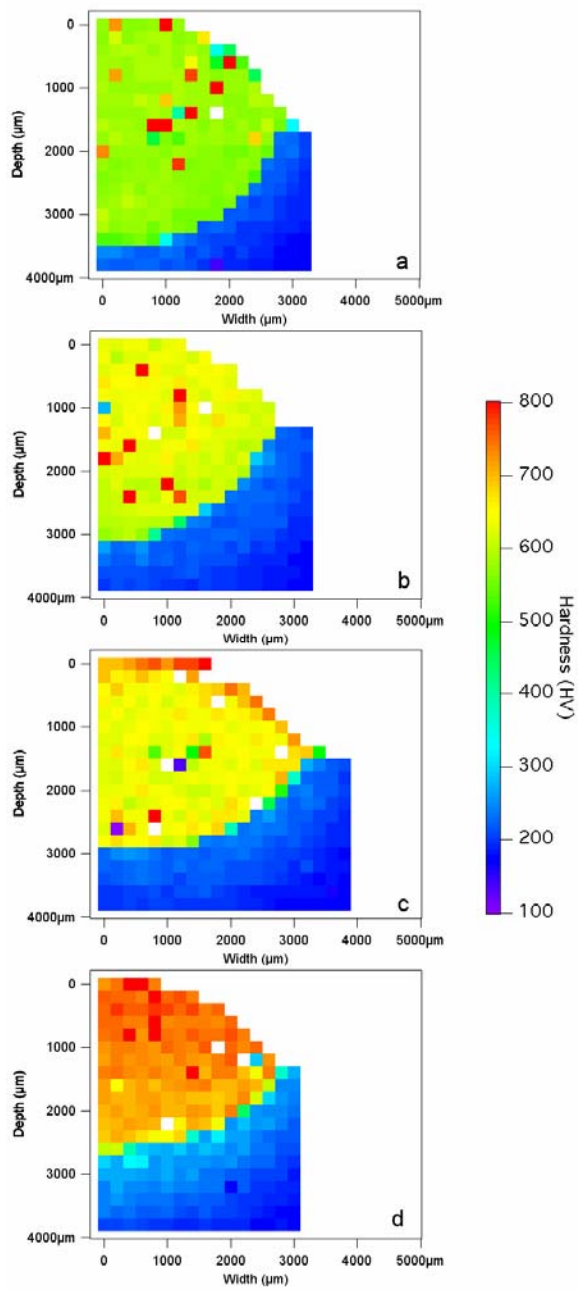

Fig. 4. Comparison of spatial hardness variations measured from one-half of the deposits made with different conditions: (*a*) 80 wt.% 431 – 20wt.%TiC – 20cfh Ar Shielding; (*b*) 80 wt.% 431 – 20 wt.% TiC – 18cfh Ar mixed with 2cfh N_2 Shielding; (*b*) 80 wt.% 431 – 20 wt.% TiC – No Shielding; and (*d*) 80 wt.% 431 – 20 wt.% TiC – 20cfh N_2 Shielding.

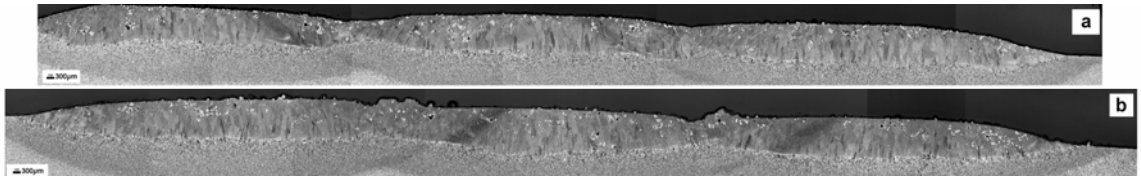

Fig. 5 Comparison of overlapping bead shapes made with diode laser source made with (*a*) argon shielding and (*b*) nitrogen shielding.

Surprisingly, the hardness of deposits increased with an increase in the nitrogen content in the shielding. Laser surface alloying with addition of TiC to 431 steel and 10-vol.% nitrogen to argon increased the hardness to 621 HV from 574 HV obtained with argon shielding. Without any intentional shielding, laser processing under air led to a hardness of 637 HV. With complete nitrogen shielding the hardness increased to 724 HV. In agreement with the initial hypothesis, it is clear that the addition of TiC and nitrogen shielding during the laser surface alloying process leads to an increase in hardness of the deposit. This is attributed to the presence of fine distribution of carbonitrides in the deposits as shown by optical microscopy. Further work is underway to evaluate the response of this microstructure during reheating and remelting that is associated with multiple bead deposits.

In the next step, the effectiveness of using shielding gas with a different laser source was evaluated under direct diode laser processing condition. The macrographs of three-layer deposits made with argon and nitrogen shielding are shown in Fig. 5. Preliminary analysis showed that both deposits were shallower compared to that of Nd-YAG laser deposits, possibly due to heat distribution of the laser source, as well as increase in scanning velocity. Interestingly, the shape of the nitrogen-shielded deposit was slightly wider and shallower than that of argon-shielded deposit, which is in agreement with the results shown in Fig. 2. The optical microstructures from these two deposits are compared in Fig. 6. The microstructures show a fine distribution of carbides in both deposits. However, the dendritic structures of carbides are well established in the case of deposits made with nitrogen shielding, as shown by arrows in Fig. 6. This result shows that the observed microstructural evolution is generic to all laser sources.

Although the above work has shown that it is possible to use computational thermodynamic models to design new laser surface alloying materials, many questions remain to be answered.

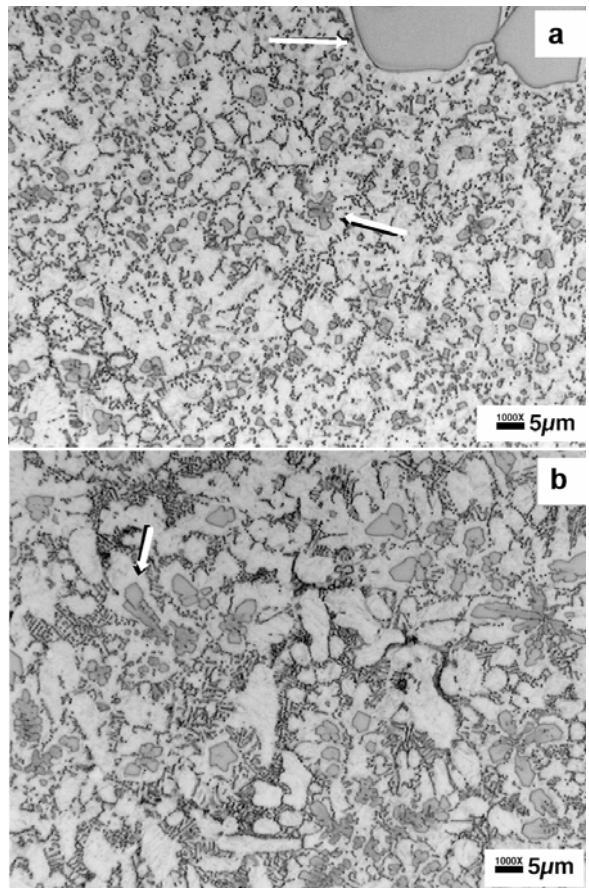

Fig. 6. Comparison of optical microstructures from the last deposit made with a direct diode laser source with (*a*) 100% argon and (*b*) 100% nitrogen shielding. The arrows show typical morphology of carbide particles.

(1) What is the maximum solubility of nitrogen that can be achieved by modifying the laser process parameters without the formation of porosity? The enhanced nitrogen dissolution due to the presence of monatomic nitrogen [27,28] in the plasma plume near the laser interaction zone must be considered. This requires detailed analysis of nitrogen pickup under different laser processing conditions and will be the focus of future work.

(2) What is the role of remelting the deposits on the stability of these carbides or carbonitrides? While remelting, these precipitates may grow either by Ostwald ripening or by collision and coalescence [29]. Therefore, the remelting and reheating processes must be controlled by avoiding excessive residence time and vigorous fluid flow.

(3) What is the role of reheating to austenite region in the heat-affected zone (HAZ) of multi-bead deposits? Will there be dissolution of carbonitrides into the austenite? Thermodynamic calculations indicate that if the carbide volume fractions are higher than the equilibrium value for a given peak temperature, they will dissolve, leading to softening. Therefore, further work is necessary to relate temporal variation of temperature at different locations in prior deposits [30,31].

Summary and Conclusions

Computational thermodynamic calculations indicated that it is possible to induce the precipitation of titanium carbonitrides during laser surface alloying provided there is a sufficient amount of dissolved titanium, carbon, and nitrogen in the liquid steel. In this research, by using a powder mixture of 431-martensitic steel, titanium carbide powder and nitrogen shielding, in conjunction with laser melting and solidification, fine distribution of titanium carbonitrides were achieved in the final deposit. The deposits showed increased hardness with an increase in nitrogen content in the shielding gas composition. The same approach was extended to direct diode laser processing and similar microstructures were attained.

Acknowledgements

Research sponsored by the Assistant Secretary for Energy Efficiency and Renewable Energy, Industrial Technologies Program, Industrial Materials for the Future, U.S. Department of Energy, under contract DE-AC05-00OR22725 with UT-Battelle, LLC. The laser processing experiments, sponsored by the Industrial Materials for the Future and by the Laser Processing Consortium, were conducted at the Applied Research Laboratory, Pennsylvania State University. The authors thank Mr. J. Tressler of the Applied Research Laboratory for producing the laser surface deposits. The authors also thank Drs. Z. Feng and Q. Han of Oak Ridge National Laboratory for helpful discussions on this paper.

References

[1]. A. Glozman and M. Bamberger *Metall. and Mater. Trans. A.*, **28A** (1996) 1699.

[2]. J. M. Pelletier, F. Oucherif, P. Sallamand, and A. B. Vannes, *Mater. Sci. Eng*., **A202**, (1995) 142.

[3]. G. Ricciardi, M. Cantello, G. Molino, W. Varani, and E. Carlet, *Key Eng. Mater*., **46**, (1990) 415.

[4]. G. Dehm, C. Scheu and M. Bamberger, Proceedings of the Conference on Laser Materials Processing, LIA, Volume **2**, (1997) F-128

[5]. I. Goldfarb and M. Bamberger *Scripta Mat*., **34**, (1996) 1051.

[6]. R. Ebner, W. Pitscheneder, R. Benes, T. DebRoy, and K. Mundra, Proceedings of the 2nd International Austria-Israel Technion Symposium and Industrial Forum, 4-6, June 1997, Graz, Austrian Technion Society, Vienna, 1997, page 79-93.

[7]. C. Zhenda, L. L. Chew and Q. Ming, *Journal of Materials Processing Technology*, **62**, (1996) 321.

[8]. J. D. Mazumdar, A. Weisheit, B. L. Mordike and I. Manna, *Mater. Sci. Eng*., **A266**, (1999) 123.

[9]. J. D. Mazumdar and I. Manna, *Mater. Sci. Eng*, **A268**, (1999) 227

[10]. J. D. Mazumdar and I. Manna, *Mater. Sci. Eng*., **A267**, (1999) 50

[11]. M. Riabkina-Fishman, and J. Zahavi, *Applied Surface Science*, **106**, (1996) 263.

[12]. C. Tassin, F. Laroudie, M. Pons and L. Lelait, *Surface and Coatings Technology*, **80**, (1996) 207.

[13]. R. Colaco, C. Pino, R. Vilar, *Scripta Materialia*, **41**, (1999) 715.

[14]. S. S. Babu, R. P. Martukanitz, K. D. Parks and S. A. David, *Metallurgical and Materials Transactions A*, **33A**, (2002) 1189.

[15]. L. F. Krivenko, *Avto. Svarka*, **1**, (1967) 6.

[16]. D. J. Kotecki and R. A. Moll, *Welding Journal*, **49**, (1970) 157s.

[17]. D. J. Kotecki and R. A. Moll, *Welding Journal*, **51**, (1972) 138s.

[18]. M. A. Quintana, J. McLane, S. S. Babu, S. A. David, *Welding Journal*, **80**, (2001) 98s.

[19]. S. S. Babu, S. A. David, and M. A. Quintana, *Welding Journal*, **80**, (2001) 91s.

[20]. I. Garcia, J. de la Fuente, and J. D. de Damborenea, *Materials Letters*, **53**, (2002) 44.

[21]. P. D. Blake, *Welding Research International*, **9,** (1979) 23.

[22]. J. O. Andersson, T. Helander, J. Hoglund and B. Sundman, *CALPHAD*, **26**, (2002) 273.
[23]. Thermotech Fe-Data Thermodynamic Database, Thermotech Ltd / Sente Software Ltd., Surrey Technology Centre, 40 Occam Road, GU2 7YG, UNITED KINGDOM
[24]. R. P. Martukanitz, Applied Research Laboratory, Unpublished research, 2003
[25]. C. R. Heiple and J. R. Roper, *Welding Journal*, **61**, (1982) S97.
[26]. A. Robert and T. DebRoy, *Metall. Mater. Trans. B.*, **32**, (2001) 941.
[27]. T. A. Palmer and T. DebRoy, *Metall. Mater. Trans. B.*, **31**, (2000) 1371.
[28]. K. Mundra and T. DebRoy, *Metall. Mater. Trans. B.*, **26**, (1995) 149.
[29]. S. S. Babu, S. A. David and T. DebRoy, *Sci. Tech. Weld. Joining*, **1**, (1996) 17.
[30]. S. M. Kelly and S. L. Kampe, *Metall. Mater. Trans. A.*, **35A**, (2004) 1869.
[31]. R. P. Martukanitz, Unpublished research, Applied Research Laboratory, 2004.